Article

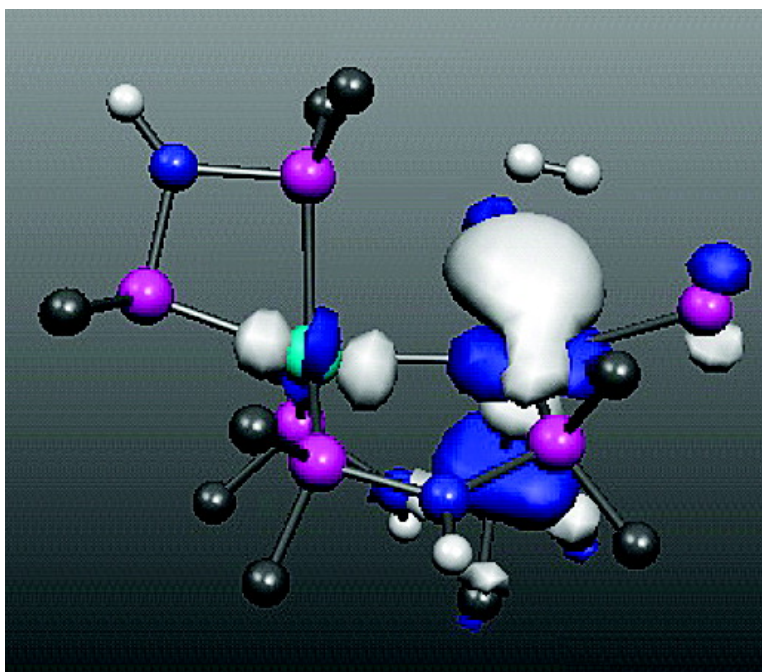# Cooperative Bimetallic Reactivity: Hydrogen Activation in Two-Electron Mixed-Valence Compounds

Thomas G. Gray, Adam S. Veige, and Daniel G. Nocera

More About This Article

Additional resources and features associated with this article are available within the HTML version:

- Supporting Information
- Links to the 5 articles that cite this article, as of the time of this article download
- Access to high resolution figures
- Links to articles and content related to this article
- Copyright permission to reproduce figures and/or text from this article

View the Full Text HTML

Cooperative Bimetallic Reactivity: Hydrogen Activation in Two-Electron Mixed-Valence Compounds

Thomas G. Gray, Adam S. Veige, and Daniel G. Nocera*

Contribution from the Department of Chemistry 6-335, Massachusetts Institute of Technology, 77 Massachusetts Avenue, Cambridge, Massachusetts 02139-4307

Received February 16, 2004; E-mail: nocera@mit.edu

Abstract: Reversible dihydrogen uptake by a two-electron mixed-valence di-iridium complex is examined with nonlocal density-functional calculations. Optimized metrics compare favorably with crystal structures of isolated species, and the calculated activation enthalpy of acetonitrile exchange is accurate within experimental error. Dihydrogen attacks the Ir_2 core at Ir^{II}; the Ir^0 center is electronically saturated and of incorrect orbital parity to interact with H_2. Isomeric η^2-H_2 complexes have been located, and harmonic frequency calculations confirm these to be potential energy minima. A transition state links one such complex with the final dihydride; calculated atomic charges suggest a heterolytic H_2 bond scission within the di-iridium coordination sphere. This investigation also establishes a ligand-design criterion for attaining cooperative bimetallic reactivity, namely, that the supporting ligand framework has sufficient mechanical flexibility so that the target complex can accommodate the nuclear reorganizations that accompany substrate activation.

Introduction

Cooperative bimetallic reactivity[1,2] is a continuing theme in inorganic chemistry, due mainly to the tenet that two metals combined might enable transformations inaccessible to single metal ions.[3,4] One commonly encounters dinuclear and higher nuclearity metal sites in Nature: in the diiron enzymes[5] soluble methane monooxygenase[6,7] and class I ribonucleotide reductase,[8,9] in the dicopper and iron−copper sites of cytochrome *c* oxidase,[10,11] in the dinickel center of urease,[12] in the O_2-transport proteins hemerythrin[5,13] and hemocyanin,[14] in the photosystem II oxygen-evolving complex,[15] in the enzymes nitrogenase,[16−18] and in nickel−carbon monoxide dehydrogenase/acetyl coenzyme A synthase[19−22] in at least a dozen zinc enzymes,[23,24] and in

certain iron−sulfur clusters,[25,26] *inter alia.*[27,28] Many of these metallobiomolecules activate small molecules by multielectron transformations. Though the precise mechanistic details of substrate activation in many such systems await disclosure, reactivity and spectroscopic studies indicate that the metals of the bioactive site may work cooperatively to activate substrates one electron at a time.[29] The protein environment, among other functions, ensures that one-electron intermediates are channeled along the desired multielectron reaction course and not diverted to nonproductive and uncontrollable one-electron/radical side reaction channels.

Such is not the case for a coordination compound. When removed from the protected environment of the protein, an exposed polynuclear metal core is subject to a variety of one-electron redox pathways that can subvert multielectron reactivity. These pathways can be circumvented when redox function is derived from metals working in concert with each other. Such intermetal redox cooperation in polynuclear metal compounds can potentially be achieved by judicious ligand design. We have explored the coordination chemistry of ligands that stabilize bimetallic centers of formal two-electron mixed valence, $M^n \cdots M^{n+2}$.[30−34] Dirhodium[35,36] and di-iridium[37,38] complexes bridged by diphosphazane ligands undergo two-electron oxida-

(1) Bosnich, B. *Inorg. Chem.* **1999**, *38*, 2554−2562.
(2) McCollum, D. G.; Bosnich, B. *Inorg. Chim. Acta* **1998**, *270*, 13−19.
(3) Fackler, J. P., Jr. *Inorg. Chem.* **2002**, *41*, 6959−6972.
(4) Halpern, J. *Inorg. Chim. Acta* **1982**, *62*, 31−37.
(5) Solomon, E. I.; Brunold, T. C.; Davis, M. I.; Kemsley, J. N.; Lee, S.-K.; Lehnert, N.; Neese, F.; Skulan, A. J.; Yang, Y.-S.; Zhou, J. *Chem. Rev.* **2000**, *100*, 235−349.
(6) Baik, M.-H.; Newcomb, M.; Friesner, R. A.; Lippard, S. J. *Chem. Rev.* **2003**, *103*, 2385−2420.
(7) Wallar, B. J.; Lipscomb, J. D. *Chem. Rev.* **1996**, *96*, 2625−2657.
(8) Stubbe, J.; van der Donk, W. *Chem. Rev.* **1998**, *98*, 705−762.
(9) Stubbe, J.; Nocera, D. G.; Yee, C. S.; Chang, M. C. Y. *Chem. Rev.* **2003**, *103*, 2167−2201.
(10) Ferguson-Miller, S.; Babcock, G. T. *Chem. Rev.* **1996**, *96*, 2889−2907.
(11) Einarsdóttir, O. *Biochim. Biophys. Acta* **1995**, *1229*, 129−147.
(12) Mobley, H. L. T.; Island, M. D.; Hausinger, R. P. *Microbiol. Rev.* **1995**, *59*, 451−480.
(13) Stenkamp, R. E. *Chem. Rev.* **1994**, *94*, 715−726.
(14) Magnus, K. A.; Ton-That, H.; Carpenter, J. E. *Chem. Rev.* **1994**, *94*, 727−736.
(15) Diner, B. A.; Rappaport, F. *Annu. Rev. Plant Biol.* **2002**, *53*, 551−580.
(16) Howard, J. B.; Rees, D. C. *Chem. Rev.* **1996**, *96*, 2965−2982.
(17) Burgess, B. K.; Lowe, D. J. *Chem. Rev.* **1996**, *96*, 2983−3011.
(18) Rees, D. C. *Annu. Rev. Biochem.* **2002**, *71*, 221−246.
(19) Dobbek, H.; Svetlitchnyi, V.; Gremer, L.; Huber, R.; Meyer, O. *Science* **2001**, *293*, 1281−1285.
(20) Drennan, C. L.; Heo, J.; Sintchak, M. D.; Schreiter, E.; Ludden, P. W. *Proc. Natl. Acad. Sci. U.S.A.* **2001**, *98*, 11973−11978.
(21) Doukov, T.; Iverson, T. M.; Seravalli, J.; Ragsdale, S. W.; Drennan, C. L. *Science* **2002**, *298*, 567−572.
(22) Darnault, C.; Volbeda, A.; Kim, E. J.; Vernède, X.; Lindahl, P. A.; Fonticella-Camps, J. C. *Nat. Struct. Biol.* **2003**, *10*, 271−279.
(23) Lowther, W. T.; Matthews, B. W. *Chem. Rev.* **2002**, *102*, 4851−4608.
(24) Lipscomb, W. N.; Sträter, N. *Chem. Rev.* **1996**, *96*, 2375−2433.
(25) Beinert, H.; Holm, R. H.; Münck, E. *Science* **1997**, *277*, 653−659.
(26) Holm, R. H.; Ciurli, S.; Weigel, J. A. *Prog. Inorg. Chem.* **1990**, *39*, 1−74.
(27) Wilcox, D. E. *Chem. Rev.* **1996**, *96*, 2435−2458.
(28) Solomon, E. I.; Chen. P.; Metz, M.; Lee, S.-K.; Palmer, A. E. *Angew. Chem., Int Ed.* **2001**, *40*, 4570−4590.
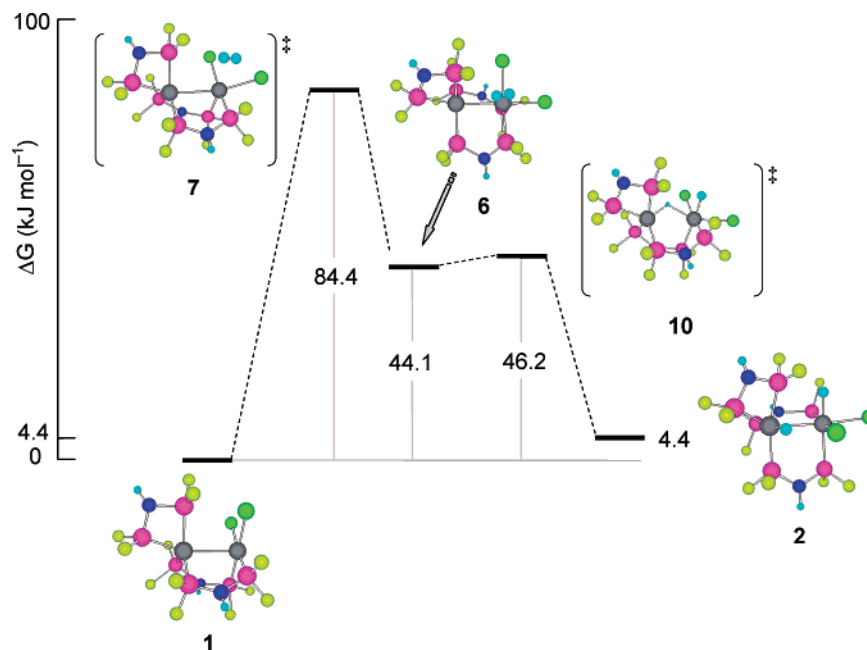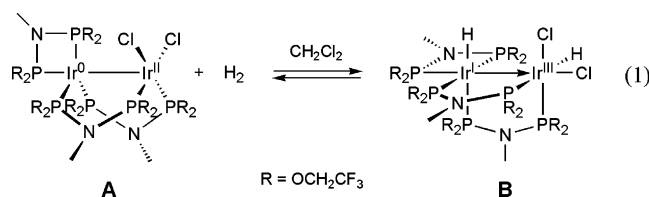(29) Holm, R. H.; Kennepohl, P.; Solomon, E. I. *Chem. Rev.* **1996**, *96*, 2239−2314.

Figure 1. Potential energy diagram relating compounds involved in the hydrogenation reaction **1** + H$_2$ → **2**. Sums of electronic and thermal free energies are indicated. Optimized geometries of reactants, products, and intermediates pertinent to the hydrogenation reaction are presented. Selected metrics for **6**: Ir−Ir, 2.780 Å; Ir−H$_2$-centroid, 1.750 Å; H−H, 0.841 Å. For transition state **7**: Ir−Ir, 2.769 Å; Ir−H$_2$-centroid, 2.994 Å; H−H, 0.743 Å; ∠(Ir−Ir−Cl)$_{av}$, 161.5°. For transition state **10**: Ir−Ir, 2.923 Å; Ir^0−H(bridge), 1.712 Å; Ir^{II}−H(bridge), 1.756 Å; Ir^I−H(terminal), 1.586 Å. Interatomic distances for reactant **1** and product **2** are provided in Table 1.

tions at the M^{n+2} center and two-electron reductions at an M^n center. With the metals working in concert, two- and four-electron transformations may be promoted along ground- and excited-state pathways.[35−37] Hydrogen production from acidic solutions is a prominent two-electron transformation promoted by these diphosphazane complexes. A Rh$_2^{0,II}$ compound [Rh$_2$(dfpma)$_3$Cl$_2$(PPh$_3$)(CO)] [dfpma = bis(difluorophosphino)-methylamine, (F$_2$P)$_2$NMe] photocatalyzes H$_2$ evolution from THF solutions of HCl and HBr.[39] In this phototransformation, H$_2$ elimination is facile and neither hydride- nor hydrido-halide intermediates are observed. This is not the case for the related di-iridium centers coordinated by the bulkier diphosphazane, tfepma [tfepma = bis(bis(trifluoroethoxy)phosphino)methylamine, MeN[P(OCH$_2$CF$_3$)$_2$]$_2$]. The increased stability of third-row metal-hydride bonds permits isolation of stable Ir$_2^{I,III}$ hydrides. For these species hydrogen elimination is thermally induced, giving rise to the unusual circumstance of reversible metal−metal bond hydrogenation without M−M bond breakage in a bimetallic compound.[37]

valence core toward efficient hydrogen production. We now report a density-functional theory study of the hydrogenation reaction, eq 1. Structural predispositions toward cooperative bimetallic reactivity are considered, and reaction intermediates and transition states are identified and related to the known reaction chemistry of the Ir$_2^{0,II}$ complex.

Results and Discussion

Figure 1 presents reactants, products, and proposed intermediates and their computed energies for the transformation shown in eq 1; for convenience, line drawings of all compounds presented in this study are provided in Chart 1. Table 1 compares calculated bond lengths of the optimized structures of the di-iridium model complexes **1** and **2** to the experimental metrics of the authentic compounds **A** and **B**, respectively. In all model complexes herein, fluorine atoms substitute for trifluoroethoxy groups on phosphorus of the tfepma ligand, and hydrogens replace *N*-methyl groups. Agreement between calculated and observed structures suggests that these simplifications are reasonable. Harmonic frequency calculations confirm the optimized structures to be energy minima. In the reactant **1**, the calculated Ir−Ir bond distance is 0.07 Å shorter than the experimental value; in dihydride product **2**, the disagreement is only 0.01 Å. This degree of accuracy is comparable to calculations of metal−metal bond lengths between fifth-period atoms using pseudopotentials or all-electron basis sets.[41−44] A survey of calculated metal−ligand and intraligand bond lengths

Owing to our interest in hydrogen-generation schemes,[39,40] we sought out properties that predispose a two-electron mixed

(30) Dulebohn, J. I.; Ward, D. L.; Nocera, D. G. *J. Am. Chem. Soc.* **1988**, *110*, 4054−4056.
(31) Dulebohn, J. I.; Ward, D. L.; Nocera, D. G. *J. Am. Chem. Soc.* **1990**, *112*, 2969−2677.
(32) Kadis, J.; Shin, Y.-g. K.; Dulebohn, J. I.; Ward, D. L.; Nocera, D. G. *Inorg. Chem.* **1996**, *35*, 811−817.
(33) Manke, D. R.; Nocera, D. G. *Inorg. Chem.* **2003**, *42*, 4431−4436.
(34) Manke, D. R.; Nocera, D. G. *Inorg. Chim. Acta* **2003**, *345*, 235−240.

(35) Heyduk, A. F.; Macintosh, A. M.; Nocera, D. G. *J. Am. Chem. Soc.* **1999**, *121*, 5023−5032.
(36) Odom, A. L.; Heyduk, A. F.; Nocera, D. G. *Inorg. Chim. Acta* **2000**, *297*, 330−337.
(37) Heyduk, A. F.; Nocera, D. G. *J. Am. Chem. Soc.* **2000**, *122*, 9415−9426.
(38) Heyduk, A. F.; Nocera, D. G. *Chem. Commun.* **1999**, 1519−1520.
(39) Heyduk, A. F.; Nocera, D. G. *Science* **2001**, *293*, 1639−1641.
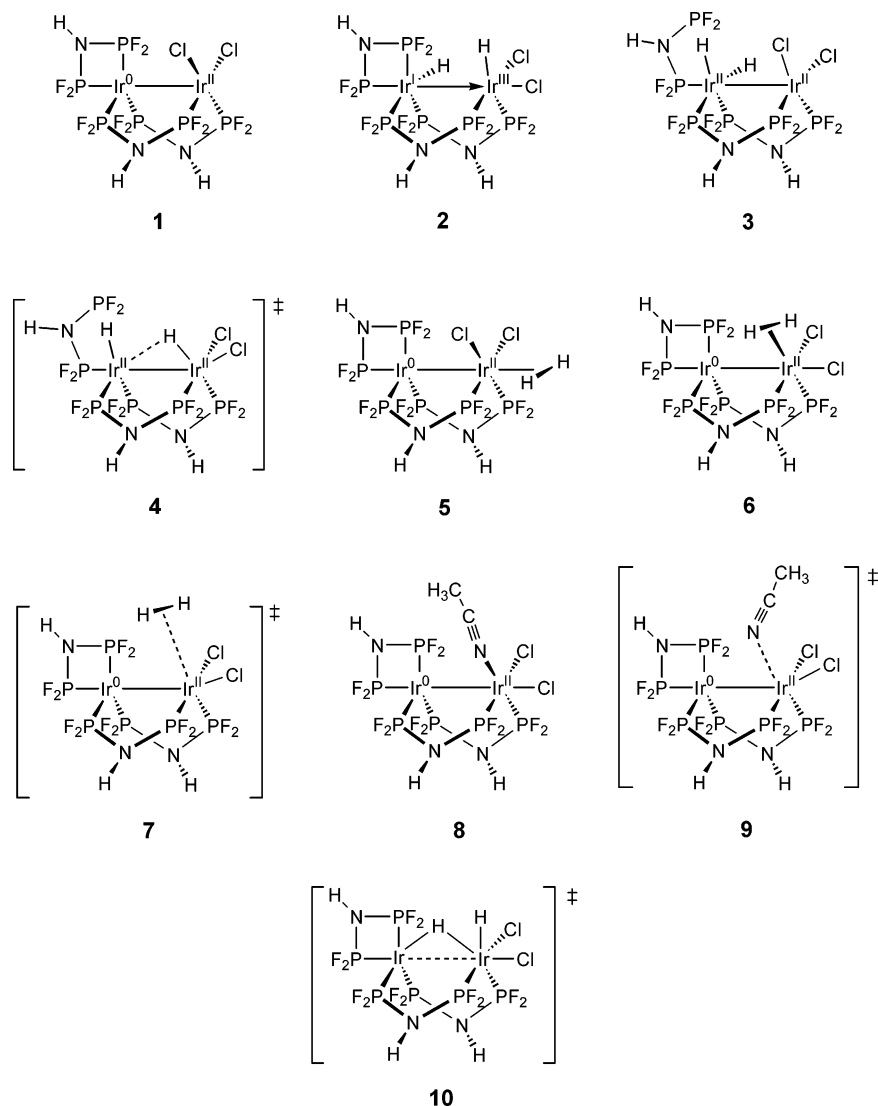(40) Nocera, D. G. *Chem. Eng. News* **2001**, *79*, 250.

Chart 1

Table 1. Calculated Bond Lengths of **1**, **2**, and **6** and Corresponding Distances Observed in **A**, **B**, and **C**, Respectively (See Supporting Information for Atom Numbering Scheme)

	1 and **A**			**2** and **B**			**8** and **C**	
bond pair	d(calcd)/Å	d(obsd)[a]/Å	bond pair	d(calcd)/Å	d(obsd)[a]/Å	bond pair	d(calcd)/Å	d(obsd)[a]/Å
Ir1−Ir2	2.721	2.7871(8)	Ir1−Ir2	2.846	2.7561(7)	Ir1−Ir2	2.767	2.7964(11)
Ir1−P9	2.298	2.2272(4)	Ir1−P9	2.247	2.271(3)	Ir1−P9	2.282	2.272(2)
Ir1−P10	2.202	2.206(4)	Ir1−P10	2.265	2.278(3)	Ir1−P10	2.227	2.272(2)
Ir1−P4	2.208	2.236(4)	Ir1−P4	2.260	2.300(3)	Ir1−P4	2.189	2.225(2)
Ir1−P7	2.225	2.278(2)	Ir1−P7	2.230	2.259(3)	Ir1−P7	2.196	2.216(2)
Ir2−Cl3	2.334	2.363(4)	Ir2−Cl3	2.394	2.511(3)	Ir2−Cl3	2.427	2.512(2)
Ir2−Cl5	2.342	2.192(4)	Ir2−Cl5	2.407	2.465(3)	Ir2−Cl5	2.393	2.427(2)
Ir2−P6	2.183	2.192(4)	Ir2−P6	2.157	2.160(3)	Ir2−P6	2.185	2.172(2)
Ir2−P8	2.182	2.189(4)	Ir2−P8	2.262	2.227(3)	Ir2−P8	2.193	2.176(2)
			Ir1−H29	1.612	1.612	Ir2−N29	2.038	2.122(7)
			Ir1−H30	1.602	1.602	N29−C30	1.141	1.104(10)

[a] From ref 37.

in the present model compounds reveals a systematic overbinding tendency, with calculated distances being ≤0.02 Å too short.

The calculated enthalpy for the hydrogenation is −42.30 kJ mol^{-1}, which includes zero-point energy, the free-energy change

is +4.10 kJ mol^{-1}. The near-thermoneutrality of the gas-phase model reaction 2

$$\mathbf{1} + H_2 \rightarrow \mathbf{2} \qquad (2)$$

concurs with the observed solvent dependence of reaction 1.

(41) Niu, S.; Hall, M. B. *J. Am. Chem. Soc.* **1999**, *121*, 3992−3999.
(42) Cotton, F. A.; Gu, J.; Murillo, C. A.; Timmons, D. J. *J. Chem. Soc., Dalton Trans.* **1999**, 3741−3745.
(43) Niu, S.; Hall, M. B. *Chem. Rev.* **2000**, *100*, 353−405.

(44) Gagliardi, L.; Roos, B. O. *Inorg. Chem.* **2003**, *42*, 1599−1603.

Table 2. Crystallographically Determined Selected Bond Lengths (Å) and Angles (deg) of $Ir_2(tfepma)_3Cl_2H_2 \cdot 3CH_3CN^a$

bond lengths		bond angles	
Ir(1)−Ir(2)	2.7464(9)	P(2)−Ir(1)−P(4)	95.02(16)
Ir(2)−Cl(1)	2.440(5)	P(2)−Ir(1)−P(6)	95.37(15)
Ir(2)−Cl(2)	2.465(4)	P(1)−Ir(2)−P(3)	100.84(17)
Ir(2)−P(1)	2.145(4)	P(4)−Ir(1)−P(5)	104.51(16)
Ir(1)−P(2)	2.286(4)	P(5)−Ir(1)−P(2)	109.48(16)
Ir(2)−P(3)	2.266(4)	P(4)−Ir(1)−P(6)	169.22(17)
Ir(1)−P(4)	2.252(4)	P(5)−Ir(1)−P(6)	69.13(15)
Ir(1)−P(5)	2.257(4)	P(5)−Ir(1)−Ir(2)	158.03(12)
Ir(1)−P(6)	2.265(4)	P(1)−Ir(2)−Cl(1)	170.26(16)
N(1S)−H(26A)	2.465	P(1)−Ir(2)−Cl(2)	86.95(16)
N(1S)−H(22A)	2.784	Cl(1)−Ir(2)−Ir(1)	90.48(11)
N(3S)−H(24A)	2.460	Cl(2)−Ir(2)−Ir(1)	167.67(12)
N(3S)−H(20B)	2.819	Cl(1)−Ir(2)−Cl(2)	86.88(16)
Ir(1)−P(2)	2.295(5)	P(1)−Ir(2)−Cl(1)	100.9(2)

^{a} Atom numbering scheme provided in Figure 2a.

The hydrogenation of **A** is reversible when performed in CH_2Cl_2 but irreversible in CH_3CN. Green-brown solutions of **A** turn yellow when the solution is charged with H_2; the solution color reverts when the H_2 atmosphere is removed from reacted solutions. Conversely, the yellow color of the product **B** persists after the H_2 atmosphere is removed from CH_3CN solutions. Not until the compound is evaporated of solvent does the green color of **A** reappear, indicating the H_2 elimination from the dihydride.

Insight into the solvent dependence is provided by X-ray structural analysis of crystals of product **B** grown from CH_2Cl_2 and CH_3CN solutions. The metric parameters of the metal complex are indistinguishable for either crystal (Table 2). However, a second coordination sphere is obtained for the metal complex when CH_3CN is the reaction medium. The asymmetric unit is comprised of **B** and three solvent molecules; as Figure 2a shows, two CH_3CN molecules are intimately associated to the chelating diphosphazane ligand bound to the Ir^0 center. Nitrogen atoms of the solvent hydrogen-bond to the aliphatic methylene protons of the chelating diphosphazane ligand. This is revealed upon viewing the structure along the di-iridium bond (Figure 2b). Aliphatic C−H⋯N contacts are usually in the range 2.522−2.721 Å.[45] The significantly shorter C−H⋯N distances of 2.46 Å (see Table 2) observed for the CH_3CN solvate of **B** attests to the strength of the H-bond contacts and their ground-state stabilization effect. The significance of the hydrogen-bond interaction appears in two habits. One is a linear hydrogen bond between the terminal hydride of the Ir1 center and a $CH_3CN(2S)$. Although this CH_3CN is 18.6 Å (N to Ir) from Ir1 within the asymmetric unit cell, a packing model reveals that it is positioned directly above an Ir1 of an adjacent molecule in the lattice at an Ir⋯N distance of 5.16 Å. The second coordination sphere solvation of the hydride appears to be an important stabilizing element, one that cannot be obtained in noncoordinating solvents such as CH_2Cl_2. A secondary stabilizing H-bond interaction appears to involve the conformation of the pendant trifluorethoxy arms of the chelating diphosphazane. In all structurally characterized Ir_2 tfepma complexes to date,[37,38] the methylene protons occur in their most sterically relaxed conformation, with methylene carbons directed away from each other. In Figure 2b, however, the methylene arms pinch inward so that the interaction of the ligand with the solvent can be established. Presumably acidity of the methylene protons is promoted by the proximity of the electron-withdrawing triflu-
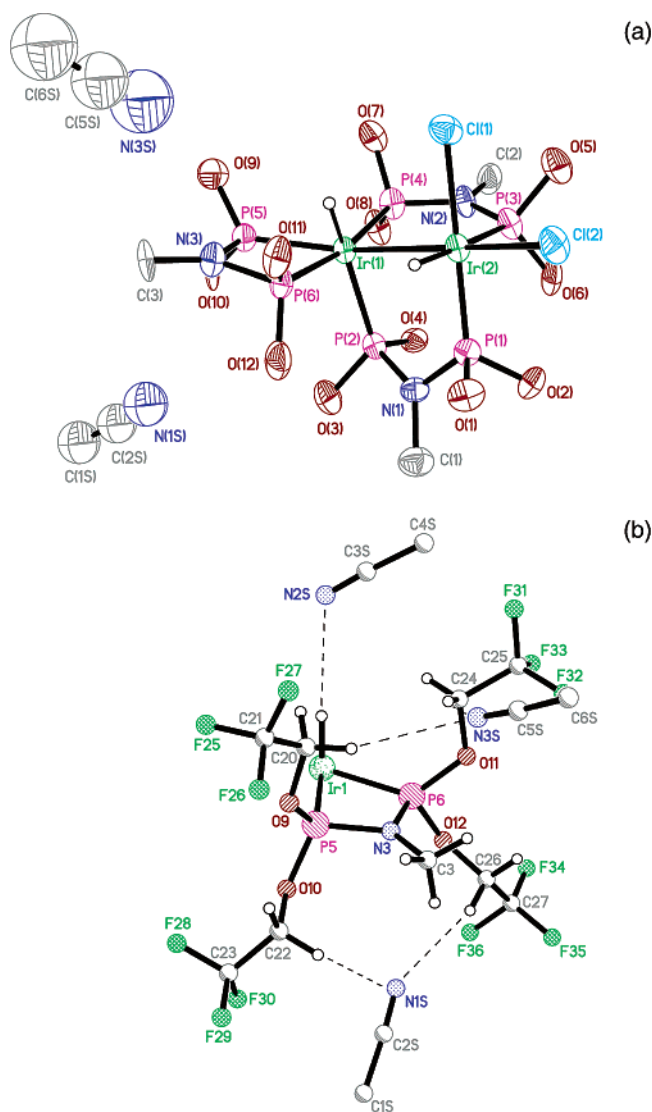
(45) Taylor, R.; Kennard, O. *J. Am. Chem. Soc.* **1982**, *104*, 5063−5070.

Figure 2. (a) Solid-state structure of $Ir_2(tfepma)_3Cl_2H_2 \cdot (CH_3CN)_3$; only the solvent molecules that directly interact with the metal complex are indicated. (b) End-on perspective of the crystal structure, highlighting the intermolecular interaction between the CH_3CNs and tfepma ligand that chelates the Ir^0 center of the di-iridium core.

oromethyl group. In solution, we suspect that such hydrogen bonding is preserved, providing additional stabilization of the dihydride product. Taken together, the two different H-bond interactions impose a kinetic barrier to H_2 elimination. By simply evaporating CH_3CN solutions of **B** (i.e., remove stabilization), **A** reforms rapidly with concomitant release of H_2. In the case of CH_2Cl_2, solvent stabilization does not appear to predominate and hence the reaction is approximated by the gas-phase calculation, which predicts a nearly thermoneutral reaction.

The dimetal hydrogenation is less remarkable thermodynamically than kinetically. Some simple organic substances, such as benzocyclobutane, have similar hydrogenation enthalpies ($\Delta H° = +5.44$ kJ mol^{-1} at 25 °C).[46] This reaction is negligible in the absence of catalysts, whereas hydrogenation of **A** is facile at room temperature and 1 atm H_2. Accordingly, the detailed investigation of this process potentially reveals reactivity principles inherent to two-electron mixed-valence dimers.

Dihydrogen Complex Formation. Hoffmann and Trinquier[47] have shown that concerted four-center addition of H_2 across a
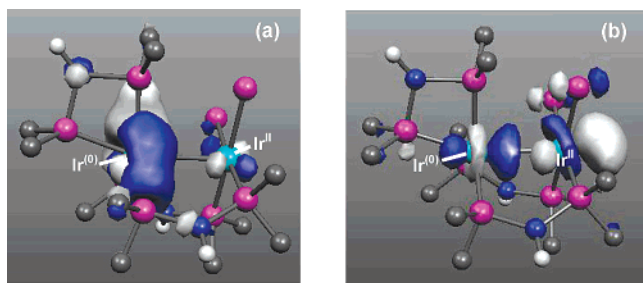
Figure 3. Calculated (a) HOMO and (b) LUMO of **1**. The isodensity value is 0.57%.

metal−metal bond is orbitally forbidden in some centrosymmetric point groups, and we have located neither intermediates nor transition states compatible with such a 1,2-addition. We therefore believe the hydrogenation of **A** to proceed by initial attack at one iridium center. Hydrogen addition to metal centers is promoted through the orbital interactions between the $1s\sigma$ and $1s\sigma^*$ orbitals of H_2 and the LUMO and HOMO of the metal complex, respectively.[48] A search was made for the appropriate η^2-H_2 adducts of the Ir^0 and Ir^{II} centers of the di-iridium core; such species are well established to precede oxidative addition at a variety of late transition metal centers.[48−50]

Figure 3 illustrates the highest-occupied and lowest-unoccupied Kohn−Sham orbitals of **1**; oxidation states of the iridium sites are indicated. The LUMO shows significant amplitude along the Ir−Ir axis; the Ir^{II} axial site is open for attack by the $1s\sigma$ orbital of H_2, but this addition is nonproductive (vide infra). The greater part of the HOMO amplitude lies on Ir^0. A nodal surface bisects the pseudo-mirror plane of the Ir^0−P−N−P chelate ring. Overlap with the $1s\sigma^*$ orbital of H_2 at the Ir^0 is parity forbidden for approach trajectories either behind or in front of the page. Moreover, attack of H_2 at the Ir^0 center is discouraged by its electronic saturation engendered by an 18-electron count. Were one phosphorus of the chelating ligand to detach, the Ir^0 center would have an electron count of 16 and might bind H_2 with both forward- and back-π donation.
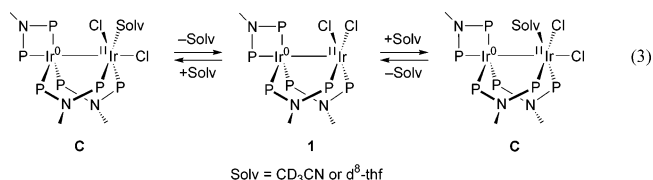
A stable structure was sought having an η^2-H_2 or two hydrides bound to Ir^0, where one arm of the chelating phosphazane is detached. Figure 4 presents one such entity, **3**; a harmonic frequency calculation shows it to be a minimum. Compound **3** is *more stable* than **2**, thus posing the question why does **B** not rearrange to an isomeric, $(H)_2Ir^{II}$−$Ir^{II}(Cl)_2$ dihydride. A transition state, **4**, links **2** and **3**; in terms of free energies, it lies 120.8 kJ mol^{-1} higher in energy than **2**. Figure 4 depicts the calculated structure of transition state **4** and its energy relative to the ground-state species. A semibridging hydride binds the non-chelated iridium in **4**, and one chloride in the transition state is near its final, axial position trans- to the Ir−Ir bond. The substantial activation barrier associated with **4** likely results from the energy needed to dissociate one arm of the chelating diphosphzane ligand from the formerly Ir^0 center; the distance to the dechelated phosphorus atom is fully 3.522 Å, and that to the semibridging hydride is 2.099 Å. A conceivable alternative

(46) Jensen, J. L. *Prog. Phys. Org. Chem.* **1976**, *12*, 189−228.
(47) Trinquier, G.; Hoffmann, R. *Organometallics* **1984**, *3*, 370−380.
(48) Kubas, G. J. *Metal Dihydrogen and σ-Bond Complexes*; Luwer Academic/Plenum: New York, 2001; p 253.
(49) Crabtree, R. H. *The Organometallic Chemistry of the Transition Metals*, 3rd ed.; Wiley-Interscience: New York, 2001.
(50) Heinekey, D. M.; Oldham, W. J., Jr. *Chem. Rev.* **1993**, *93*, 913−926.

mechanism is a stepwise sequence, where phosphazane dechelation precedes H-transfer. Exploratory calculations indicated that decomplexation of the equatorial phosphorus of the chelating phosphazane raised the energy monotonically, with no indication of a stable "arm off" minimum. Attempts to optimize such structures collapsed to the optimized structure of **2**. These findings are consistent with the substitutional inertness of third-row transition metal centers.[51,52] Overall, these model calculations suggest that the experimental dihydride is only kinetically stable, with a prohibitive barrier to a dissociative isomerization. Given the parity-forbiddenness of H_2 attack on the 18-electron, coordinatively intact Ir^0 center, the substantial energy required for dissociation of a diphosphazane ligand, and the experimental structure of dihydride **B**, we dismiss the possibility that H_2 first attacks at Ir^0.

Two isomeric minima, **5** and **6**, both with H_2 η^2-bound to Ir^{II}, were located, respectively. In adduct **5**, H_2 is dihapto-bound trans to the metal−metal bond; in **6**, it is cis. Adduct **6** is calculated to be 14.6 kJ mol^{-1} less stable than **5**, which is 25.1 kJ mol^{-1} more energetic than dihydride **2**. Attempts to optimize an Ir^0−$Ir^{IV}(H)_2$ dihydride converged to the η^2-dihydrogen structures **5** and **6**; thus, the presence of an Ir^{IV} addition product does not appear to be germane to the two-electron mixed valence chemistry reported here.

The LUMO is metal−metal σ-antibonding (Figure 3b); overlap with the H_2 $1s\sigma$ orbital is parity allowed. H_2 addition at the axial site of the Ir^{II} center (trans to the metal−metal bond) is nonproductive. The H−H distance within the bound H_2 is 0.791 Å in **5**, similar to that of free H_2 ($d_{calcd} = 0.738$ Å). The H_2 bond elongates to 0.841 Å when it resides in the equatorial coordination site of **6**. Moreover, the Ir^{II}−H_2-centroid distance in **6** is shorter than that for **5** (1.750 Å in **6**, 1.911 Å in **5**). Clearly, the bound η^2-H_2 in **6** is more extensively activated than that in **5**. A transition state (**7**) for binding η^2-H_2 in the cis position of the Ir^{II} center has been located. An Ir^{II}−H_2 midpoint distance of 2.994 Å and H−H separation of 0.743 Å indicate that the dihydrogen σ-bond is minimally perturbed in the transition state. The LUMO of transition state **7** (Figure 5) shows considerable amplitude on Ir^{II} and is suitably disposed to receive electron-donation from the $1s\sigma$ orbital of H_2 as the primary donor−acceptor interaction. Transition state **7** lies 84.4 kJ mol^{-1} in energy above **1** + H_2 and 40.3 kJ mol^{-1} above dihydrogen adduct **6**. Figure 6a illustrates the imaginary-frequency vibration, calculated at $118i$ cm^{-1}, for **7**. The trajectory of H_2 approach is clearly visible as is the motion of the equatorial chloride toward its axial position observed experimentally in **B**.

The computed association of η-H_2 to **A** concurs with experimental findings for the addition of simple two-electron donors. Variable temperature NMR studies[37] have identified the following exchange process,

$$\text{(3)}$$

Solv = CD$_3$CN or d^8-thf

As observed for η^2-H_2 addition, the donor ligand adds to the equatorial site of the Ir^{II} center. For Solv = CH$_3$CN, adduct **C** has been structurally verified.[37] Moreover, the calculated
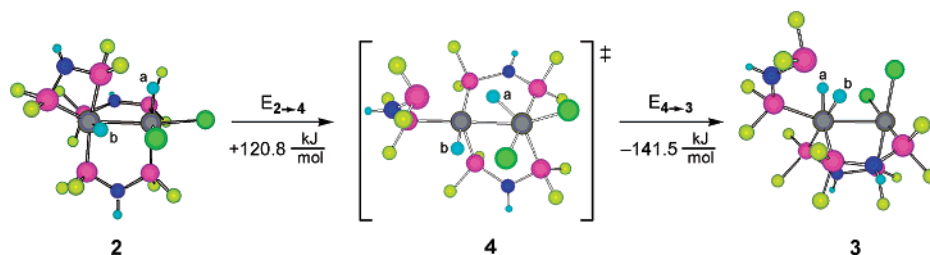
Figure 4. Reaction profile relating Ir^{II}–Ir^{II} nonchelated model dihydride **3**, which corresponds to no observed iridium complex, to the known dihydride product **2** via the located transition state **4**. Metal-bound hydrogens are labeled for clarity; the hydrogen labeled a is the one that transfers. Selected interatomic distances of **3**: Ir–Ir, 2.711 Å; Ir–H, 1.601 and 1.605 Å; Ir–P(unligated), 3.719 Å; Ir–P(ligated), 2.188 Å; H–H, 2.212 Å. Selected interatomic distances of transition state **4**: Ir–Ir, 2.617 Å; Ir^{I}–H(bridge), 2.099 Å; Ir^{III}–H(bridge), 1.728 Å; Ir–H(terminal), 1.600 Å; Ir–P(unligated), 3.522 Å; Ir–P(ligated), 2.217 Å.
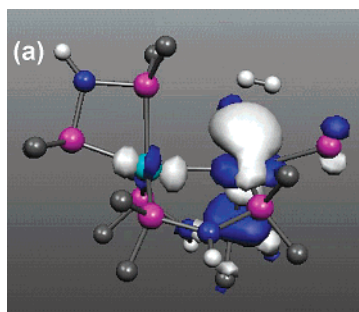

Figure 5. LUMO-1sσ donor–acceptor interaction of transition state **7** and H$_2$.

activation energy for η^2-H$_2$ addition (84.4 kJ mol^{-1}) is similar to the observed activation parameters for CD$_3$CN ($\Delta H^{\ddagger} = 105 \pm 17$ kJ mol^{-1}) and THF ($\Delta H^{\ddagger} = 54 \pm 4$ kJ mol^{-1}) exchange.[37] We sought to reference our calculations for ligand association to the Ir$_2^{0,II}$ core by determining the energetics of eq 3 for CH$_3$CN exchange. Figure 7 illustrates a geometry-optimized model of the known acetonitrile adduct Ir$_2^{0,II}$(tfepma)$_3$Cl$_2$-(MeCN) (**8**) (Table 1 presents a comparison to crystallographic metrics) and the transition state (**9**) located for solvent exchange. A frequency calculation confirms **9** to be a saddle-point of the potential energy surface. Animation of the single imaginary vibration, Figure 6b, confirms significant motion coupled with CH$_3$CN departure. Note that the two transition structures of the η^2-H$_2$ and CH$_3$CN adducts are qualitatively much alike and the motion of the ligands in each of the transition states is similar. The distance between the acetonitrile nitrogen and the nearer iridium is 3.252 Å, a prediction consistent with the dissociative character found experimentally. The calculated activation energy is 82.5 kJ mol^{-1}, in quite fair agreement with the experimental number and similar to that observed for η^2-H$_2$; correction for zero-point energy with addition of thermal free energy (at 298.15 K) yields an activation free energy of 92.8 kJ mol^{-1}, which is within the experimental error of the observed value for CH$_3$CN exchange. The nearness of computed energies to experimental findings establishes the validity of the computational approach herein.

Bound-Dihydrogen Activation. Once residing in the equatorial coordination site, η^2-H$_2$ is readily activated to dihydride **2** via transition state **10**. A harmonic frequency calculation confirms **10** to be an energy maximum with one imaginary frequency; an intrinsic reaction coordinate[53,54] connects **6**, **2**, and **10**. In terms of free energies, **10** is 41.8 kJ mol^{-1} less stable than product **2**, and 2.0 kJ mol^{-1}, less stable than intermediate **6**. As expected, a hydride bridges the iridium centers; the other

hydride resides at the onetime Ir^{II} (Ir^{III} in **2**). Figure 8 animates the imaginary frequency of **10**; significant vibrational amplitude is visible for the bridging hydrogen. What is counterintuitive is the distention of the Ir–Ir bond in **10**; at 2.923 Å, it is some 0.202 Å longer than the analogous bond length calculated for **1**, and 0.177 Å longer than the same bond in **2**. It is easily the longest metal–metal bond in any of the structures calculated here.

We note that the H$_2$ addition results reported here are related to those of Stanley and collaborators,[55–59] who have shown that dihydrogen is readily activated by dirhodium tetraphosphine complexes. In these systems, initial oxidative addition of H$_2$ to a single Rh^{I} center affords a two-electron mixed valence Rh^{I}–Rh^{III} intermediate that undergoes hydride migration to the final Rh^{II}–Rh^{II} dihydride, presumably through an intermediate bridged hydride.

Table 3 collects Mulliken atomic charges calculated for η^2-H$_2$ complex **8**, transition state **10**, and product **2**. The dissimilar iridium ion charges reflect the mixed valency of these complexes. The calculated charges also indicate a very polarized, almost heterolytic splitting of the H$_2$. The η^2-H$_2$ in **6** is significantly polarized with the H closer to Ir^{0} exhibiting the higher positive charge. The more positively charged hydrogen is attached to the lower-valent iridium (Ir^{I} in **2**), indicating that this Ir–H bond is more ionic than the Ir^{III}–H bond.

Mechanical Predispositions to Cooperative Bimetallic Reactivity. Activated complex **10** lies only 2.0 kJ mol^{-1} above **6**; its easy accessibility accounts for the ready, reversible hydrogenation seen experimentally. Substantial deformation energy might be expected for stretching a metal–metal bond (from 2.780 in **6** to 2.923 Å in **10**) bridged by two phosphazane ligands, and the ligand bridges necessarily moderate the hydrogenation's ease and reversibility.

Table 4 assembles the lowest-energy vibrational frequencies for scissor and bending modes calculated for two pertinent phosphazane ligands and for acetate, a representative bridging

(51) Dunand, F. A.; Helm, L.; Merbach, A. E. *Adv. Inorg. Chem.* **2003**, *54*, 1–71.
(52) Burgess, J.; Hubbard, C. D. *Adv. Inorg. Chem.* **2003**, *54*, 72–157.
(53) Gonzalez, C.; Schlegel, H. B. *J. Chem. Phys.* **1989**, *90*, 2154–2161.
(54) Gonzalez, C.; Schlegel, H. B. *J. Phys. Chem.* **1990**, *94*, 5523–5527.
(55) Broussard, M. E.; Juma, B.; Train, S. G.; Peng, W.-J.; Laneman, S. A.; Stanley, G. G. *Science* **1993**, *260*, 1784–1788.
(56) Carter, R. D.; Howell, D. K.; Peng, W.-J.; Train, S. G.; Treleaven, W. D.; Stanley, G. G. *Angew. Chem., Int. Ed. Engl.* **1996**, *35*, 2253–2256.
(57) Peng, W.-J.; Train, S. G.; Howell, D. K.; Fronczek, F. R.; Stanley, G. S. *Chem. Commun.* **1996**, 2607–2608.
(58) Laneman, S. A.; Fronczek, F. R.; Stanley, G. G. *J. Am. Chem. Soc.* **1988**, *110*, 5585–5586.
(59) Stanley, G. In *Catalysis by Di- and Polynuclear Metal Cluster Complexes;* Adams, R. D., Cotton, F. A., Eds. Wiley-VCH: New York, 1998; pp 345–372.
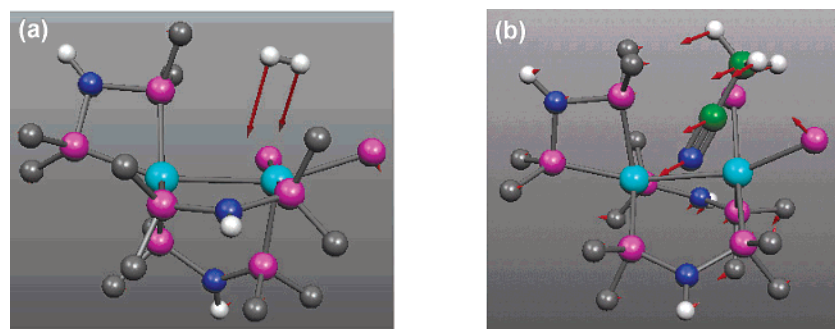
Figure 6. Depiction of the imaginary-frequency vibrational mode calculated for transition states of the addition of two-electron donors (a) η^2-H_2 and (b) CH_3CN to **2**.
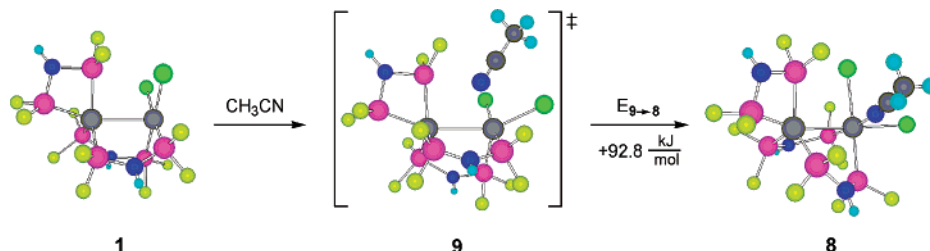

Figure 7. Geometry-optimized model of the known acetonitrile adduct **8** and reaction profile accounting for the energetics of acetonitrile exchange at the Ir^0–Ir^{II} core. Interatomic distances for reactant **1** and **8** are provided in Table 1. Selected interatomic distances of transition state **9**: Ir–Ir, 2.769 Å; Ir^{II}–$NCCH_3$, 3.252 Å.
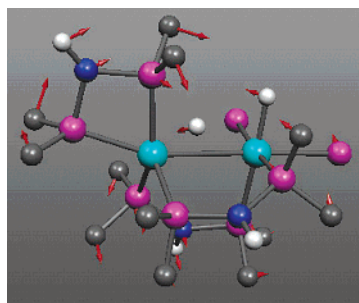

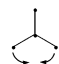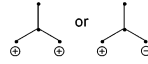**Figure 8.** Depiction of the imaginary-frequency vibrational mode calculated for **10**.

Table 3. Mulliken Electrostatic Charges Calculated for **6**, **10**, and **2**

atom	charge		
	6	**10**	**2**
Ir(chelated)	−2.325	−2.583	−2.793
Ir(nonchelated)	−1.652	−1.632	−1.456
H(chelated Ir)[a]	0.1308	0.2489	0.3345
H(nonchelated Ir)[b]	0.2598	0.1820	0.1151

[a] For compound **6**, H oriented toward Ir^0; for compound **10**, H is bridging; for compound **2**, terminal H on Ir^I. [b] For compounds **6**, **2**, and **10**, terminal H on nonchelated Ir.

ligand for metal–metal bonded complexes. These modes provide some measure of the flexibility of the ligand backbone. The tabulated frequencies employ the 6-31G(d,p) basis set used for ligand atoms of **1**–**10** and are unscaled. The ligand dfpa is the model phosphazane used for calculations herein. Dfpma is its *N*-methyl derivative and figures extensively in the related rhodium chemistry. The table shows the phosphazane backbone to be floppy relative to acetate. The ancillary phosphazanes all undergo a large distortion for a small energy input, unlike the more common bridging ligand, acetate. Carboxylates and related ligands bridge a great multitude of metal–metal bonded dimers[60,61] but also rigidify them. Cooperative bimetallic

Table 4. Modes for Scissor and Out-of-Plane Bending Vibrations Calculated for Bidentate Phosphazanes and for Acetate

Type of mode	dfpma, C_s PF_2–N–PF_2		dfpa, C_{2v} H–N, PF_2–PF_2		acetate, C_s	
	mode	ν / cm^{-1}	mode	ν / cm^{-1}	mode	ν / cm^{-1}
Scissor	A′	183	A_1	169	A″	647
	A′	262	A_1	258	A′	916
	A′	426	A_1	423	A′	1463
	A′	912	A_1	892		
Out-of-plane bending	A″	66	A_2	48	A″	627
	A″	277	B_2	54	A″	1062
	A″	874	A_2	272		
	A′	883	A_2	888		

reactivity is rare in such compounds, possibly because the ligands are mechanically constraining. Indeed, small molecule activation at bimetallic centers bridged by carboxylate is often promoted only when one arm of the rigid carboxylate dissociates from the bimetallic center (aka, the carboxylate-shift mechanism).[62] Bosnich[1,2] has argued that poorly designed, inflexible ligands can forestall bimetallic reactivity, even without direct bonds joining the metal centers. The results reported here support Bosnich's contention of the importance of mechanical coupling to reactivity at bimetallic centers.

The foregoing results establish low-energy ligand flexing modes as important adjuncts to cooperative reactivity between metal centers. This property is especially pertinent for metal centers that differ by more than one electron, since significant reorganization of the primary coordination environment must typically accompany this difference in formal oxidation states.

(60) Cotton, F. A.; Walton, R. A. *Multiple Bonds between Metal Atoms*; Oxford University Press: New York, 1993.
(61) Cotton, F. A. *Inorg. Chem.* **1998**, *37*, 5710−5720.
(62) Rardin, R. L.; Tolman, W. B.; Lippard, S. J. *New J. Chem.* **1991**, *15*, 417.

This is the case for the reactants, products, and intermediates on the potential energy surface of Figure 1. The ability to flex bridging and chelating phosphazane ligands with only a modest energy input reaction appears to be important to the facile addition and elimination of hydrogen from the Ir^0-Ir^{II} core.

Conclusions

The geometry-optimized two-electron mixed-valence complex **1** and correspondent observed complex **A** are composite structures of metals in formal oxidation states that differ by two. A coordinatively (CN = 5) and electronically saturated (18 e⁻) Ir^0 center is joined to a coordinatively (CN = 4) and electronically (16 e⁻) unsaturated Ir^{II} center. Hydrogen addition occurs at the Ir^{II} end of the molecule to produce dihydride **2**. The hydrogenation is predicted to be nearly thermoneutral, consistent with the reversible hydrogenation of the experimental compound **A** in nonhydrogen-bonding solvents. The observed product, **B**, is thermodynamically unstable compared to an isomer having two hydrides on one iridium site (**3**). However, this isomerization reaction is kinetically impeded (**4**), with a calculated barrier of 120.8 kJ mol⁻¹, and is not observed experimentally. Hydrogenation is initiated by side-on attack at an equatorial coordination site (**6**); attack at the available axial coordination site (**5**), although of less energy, is unproductive. The crucial equatorial coordination site is opened by a shift of a chloride from an equatorial to an axial coordination position; this ligand motion imposes the largest barrier to the reversible hydrogenation of the Ir^0-Ir^{II} core. This rate-limiting step is also the first step in the proposed reaction sequence. The energy of this barrier is consistent with that measured experimentally for the reversible addition of other two-electron donor ligands (e.g., CH_3CN) to the Ir^0-Ir^{II} activation barriers. An Ir^0-Ir^{IV} dihydride does not appear to be important to the reaction pathway, as geometry optimization of such species collapse to one of the two η^2-H_2 complexes. Once residing in the equatorial coordination site, the η^2-H_2 complex smoothly converts to the dihydride in an elementary reaction. Transition state **10**, which was confirmed by harmonic frequency and intrinsic reaction coordinate calculations, is virtually isoenergetic with **8**.

Transition state **10** bears a much-elongated Ir–Ir bond compared to every other optimized structure herein and also relative to the experimental bond lengths of near-analogue compounds. The small energy barrier suggests a flexible complex, with no great distortion penalty imposed by the ligands. Vibrational frequency calculations find numerous low-frequency normal modes for the phosphazane ligands. In particular, the symmetric P–N–P shearing mode has significantly lower energy than the corresponding vibrations in carboxylates. These results imply that a small energy input elicits a large distortion and that distention of the bimetallic core is unhindered by the phosphazane bridges in these complexes. In addition to its pliability, spectroscopic and structural studies show that the stereoelectronic properties of the diphosphazane framework can sustain two-electronic mixed valence character.[33,35,37] Thus the ligand is able to accommodate the two-electron mixed valence character of the bimetallic core during the course of the reaction through the transition state:

Large reorganizations of the primary coordination sphere of the di-irdium complex are therefore not required for the reversible addition and elimination of H_2. These electronic and steric properties of the ligand appear to be advantageous, if not compulsory, to the cooperative bimetallic and reversible activation of H_2 at a two-electron mixed valence core.

Experimental Section

General Procedures. All synthetic manipulations were conducted in the dry, anaerobic environment provided by a Schlenk-line or by a nitrogen-filled glovebox. Solvents for synthesis were of reagent grade or better and were dried according to standard methods.[63] The ligand precursor $MeN(PCl_2)_2$,[64,65] and the diphosphazane ligand (tfepma) and di-iridium complex $Ir_2^{0,II}(tfepma)_3Cl_2$ were prepared following published procedures.[37] The starting materials [Ir(cod)Cl]₂ (Strem) and H_2 (BOC Gases, UHP Grade 5) were used as received.

Reaction of A with H_2 To Give $(tfepma)_3Ir_2Cl_2H_2\cdot3CH_3CN$ (B). To a degassed orange solution of **A** (500 mg, 0.261 mmol) in CH_3CN (10 mL) was admitted 1 atm H_2 (g). After 15 min of stirring at ambient temperature, the solution turned yellow. The yellow color remained after H_2 was removed and the solvent condensed to 1 mL. Recrystallization from a CH_3CN/CH_2Cl_2 (2 mL) solution layered with pentane (5 mL) resulted in pale-yellow X-ray quality crystals after 5 days. ¹H NMR (500 MHz, CD₃CN, 25 °C), δ/ppm: −11.63 (dq, 188 Hz, 16.0 Hz, 1 H), −8.17 (d, 278 Hz, 1 H), 2.81 (t, 7.37 Hz, 6 H), 4.2−5.7 (m, 24 H). ³¹P{¹H} NMR (202.5 MHz, CD₃CN, 25 °C) δ/ppm: 17.85 (s, 1 P), 45.26 (d, 746 Hz, 1 P), 71.34 (d, 159 Hz, 1 P), 86.84 (d, 155 Hz, 1 P), 95.50 (dd, 752 Hz, 218 Hz, 1 P), 99.40 (d, 222 Hz, 1 P). IR (KBr) ν_{Ir-H}/cm⁻¹: 2053, 2071.

X-ray Structure of $(tfepma)_3Ir_2Cl_2H_2\cdot3CH_3CN$ (B). A 0.40 mm × 0.29 mm × 0.28 mm crystal was taken from a batch of crystals grown from a 1:1 mixture of CH_2Cl_2/CH_3CN, and the compound was layered with pentane at −30 °C. The crystal was coated in Paratone N oil and mounted onto a glass fiber. A total of 25 493 reflections were collected in the θ range 2.19° to 23.31°, of which 9759 were unique (R_{int} = 0.0532). The structure was solved by direct methods using standard Fourier techniques. One ligand trifluoroethoxy group was disordered and refined isotropically with the command DFIX used to restrain bond distances. Solvent molecules were also refined isotropically due to their high thermal motion in the crystal lattice at 193 K. The Ir−H hydrides were not located in the difference Fourier map. All other hydrogen atoms were placed in calculated positions using a standard riding model and were refined isotropically. The largest peak and hole in the difference map were 4.780 and −2.610 eÅ⁻³. The least squares refinement converged normally giving residuals of R_1 = 0.0919, wR_2 = 0.2049, and GOF = 1.284. The crystal data for $C_{33}H_{44}Cl_2F_{36}Ir_2N_6O_{12}P_6$: monoclinic $P2_1/n$, Z = 4, a = 12.3635(15) Å, b = 23.491(3) Å, c = 23.867(3) Å, β = 99.908(2)°, V = 6828.3(14) Å³, ρ_{calc} = 1.984 Mg/m³, $F(000)$ = 3920.

Computational Details. Calculations were performed within the Gaussian 98 program suite.[66] DFT computations employed the hybrid functional of Truhlar et al.,[67] which is a variant of the Perdew−Wang exchange-correlation functional[68−71] incorporating a 42.8% admixture of Hartree−Fock exchange. The default "extrafine" grid was used throughout. Self-consistent field convergence was achieved with direct methods. Equilibrium geometries were optimized in redundant internal coordinates;[72] transition state structures were computed with quadratic synchronous searching algorithms.[73] Relativistic effective core potentials were used for iridium along with the standard Hay−Watt[74] double-ζ basis set, augmented by the optimized Ir 6p-function of Couty and Hall.[75] The 6-31G(d,p) basis of Pople and co-workers[76,77] was applied

                                                                         (4)

(63) Armarego, W. L. F.; Perrin, D. D. *Purification of Laboratory Chemicals*, 4th ed.; Butterworth-Heinemann: Oxford, 1996.
(64) Nixon, J. F. *J. Chem. Soc. A* **1968**, 2689−2692.
(65) King, R. B.; Gimeno, J. *Inorg. Chem.* **1978**, *17*, 2390−2395.

to all other atoms. Reported energies are sums of electronic and thermal free energies. As such, they are therefore corrected for zero-point energies. Thermodynamic quantities were computed using unscaled vibrational frequencies, in the manner encoded in Gaussian 98. The minimum of the electronic energy hypersurface is used to compute vibrational partition functions and all electronic excited states are assumed to be energetically inaccessible. Translational entropy changes that accompany changes in the number of moles of gases during the reaction are included. We report herein gas-phase calculations, and no attempt has been made to correct for the nonideality of gases, nor for effects of solvation. All calculations were spin-restricted, and geometry optimizations proceeded without imposed symmetry. Canonical Kohn−Sham orbitals were imaged with the program Molekel;[78,79] default isodensity values were applied.

Supporting Information Available: Atom numbering schemes for compounds **1**−**10** and tables of crystal data, atomic coordinates, bond lengths and angles, anisotropic thermal parameters, and hydrogen coordinates for $(tfepma)_3Ir_2^{0,II}H_2Cl_2 \cdot 3CH_3CN$ (**B**) (27 pages/PDF). An X-ray crystallographic file for $(tfepma)_3Ir_2^{0,II}H_2Cl_2 \cdot 3CH_3CN$ (**B**), in CIF format. This material is available free of charge via the Internet at http://pubs.acs.org.

JA0491432

(66) Frisch, M. J.; Trucks, G. W.; Schlegel, H. B.; Scuseria, G. E.; Robb, M. A.; Cheeseman, J. R.; Zakrzewski, V. G.; Montgomery, J. A., Jr.; Stratmann, R. E.; Burant, J. C.; Dapprich, S.; Millam, J. M.; Daniels, A. D.; Kudin, K. N.; Strain, M. C.; Farkas, O.; Tomasi, J.; Barone, V.; Cossi, M.; Cammi, R.; Mennucci, B.; Pomelli, C.; Adamo, C.; Clifford, S.; Ochterski, J.; Petersson, G. A.; Ayala, P. Y.; Cui, Q.; Morokuma, K.; Malick, D. K.; Rabuck, A. D.; Raghavachari, K.; Foresman, J. B.; Cioslowski, J.; Ortiz, J. V.; Stefanov, B. B.; Liu, G.; Liashenko, A.; Piskorz, P.; Komaromi, I.; Gomperts, R.; Martin, R. L.; Fox, D. J.; Keith, T.; Al-Laham, M. A.; Peng, C. Y.; Nanayakkara, A.; Gonzalez, C.; Challacombe, M.; Gill, P. M. W.; Johnson, B. G.; Chen, W.; Wong, M. W.; Andres, J. L.; Head-Gordon, M.; Replogle, E. S.; Pople, J. A. *Gaussian 98*, revision A.9; Gaussian, Inc.: Pittsburgh, PA, 1998.

(67) Lynch, B. J.; Fast, P. L.; Harris, M.; Truhlar, D. G. *J. Phys. Chem.* **2000**, *104*, 4811−4815.

(68) Perdew, J. P. In *Electronic Structure of Solids '91*; Ziesche, P., Eschig, H., Eds.; Akademie Verlag: Berlin, 1991.

(69) Perdew, J. P.; Chevary, J. A.; Vosko, J. H.; Jackson, K. A.; Pederson, M. R.; Singh, D. J.; Fiolhais, C. *Phys. Rev. B* **1992**, *46*, 6771−6787.

(70) Perdew, J. P.; Burke, K.; Wong, Y. *Phys. Rev. B* **1996**, *54*, 16533−16539.

(71) Burke, K.; Perdew, J. P.; Wang, Y. In *Electronic Density Functional Density Theory: Recent Progress and New Directions*; Dobson, J. F., Vignale, G., Das, M. P., Eds.; Plenum: New York, 1998.

(72) Peng, C.; Ayala, P. Y.; Schlegel, H. B.; Frisch, M. J. *J. Comput. Chem.* **1996**, *17*, 49−56.

(73) Peng, C.; Schlegel, H. B. *Israel J. Chem.* **1993**, *33*, 449−454.

(74) Hay, P. J.; Wadt, W. R. *J. Chem. Phys.* **1985**, *82*, 270−283, 284−298, 299−310.

(75) Couty, M.; Hall, M. B. *J. Comput. Chem.* **1996**, *17*, 1359−1370.

(76) Hariharan, P. C.; Pople, J. A. *Theor. Chim. Acta* **1973**, *28*, 213−222.

(77) Francl, M. M.; Pietro, W. J.; Hehre, W. J.; Binkley, J. S.; Gordon, M. S.; DeFrees, D. J.; Pople, J. A. *J. Chem. Phys.* **1982**, *77*, 3654−3655.

(78) Flükiger, P.; Lüthi, H. P.; Portmann, S.; Weber, J. *MOLEKEL 4.3*; Swiss Center for Scientific Computing: Manno, Switzerland, 2000−2002.

(79) Portmann, S.; Lüthi, H. P. MOLEKEL: An Interactive Molecular Graphics Tool. *Chimia* **2000**, *54*, 766−770.